Optimal Yaw-Rate Control for Electric Vehicles with Active Front-Rear Steering and Four-Wheel Driving-Braking Force Distribution

Hiroshi Fujimoto and Kenta Maeda
The University of Tokyo
5-1-5, Kashiwanoha, Kashiwa, Chiba 227-8561 Japan
Email: fujimoto@k.u-tokyo.ac.jp

***Abstract*—Direct yaw-moment control (DYC) is an effective method for achieving stable vehicle motion. In the DYC systems of vehicles with in-wheel motors and active front and rear steering systems, some control inputs are generally redundant. This means that input variables cannot be decided uniquely to control each longitudinal, lateral, and yawing motion. The equalization of workloads of each wheel based on longitudinal and lateral force distributions enhances the cornering performance of vehicles. Therefore, we propose a method for obtaining longitudinal- and lateral-force distributions based on least-squares solutions of the equations of longitudinal, lateral, and yawing motions. Furthermore, we propose a lateral-force control method using tire lateral force sensors, active front and rear steering systems, and a DYC method for enhancing the yaw-rate control performance. In this study, through simulations and experiments, we show that the equalization of the workload on each wheel and quick yaw-rate response are achieved by adopting the proposed methods.**

I. Introduction

As a solution for energy and environmental problems, the electric vehicle (EV) has been receiving significant attention. In addition, EVs have many advantages over internal combustion engine vehicles owing to the use of electric motors and inverters in EV drivetrains. These advantages can be summarized as follows [1]:

1) The torque response of electric motors is 10–100 times faster than that of internal combustion engines.
2) All wheels can be controlled independently by using in-wheel motors.
3) The output torque of an electric motor can be measured accurately from the motor current.
4) Braking force can be generated by regeneration as well.

In the field of vehicle dynamics and control, many studies on yaw-rate control have been reported for stabilizing vehicles' cornering motions. For ICEVs without a torque-distribution mechanism and EVs without in-wheel motors, active front and rear systems are used for controlling the yaw rate [2]. In contrast, for EVs with all-wheel independent drive systems such as in-wheel motors, yaw-rate control methods have been studied based on the active yaw moment generated owing to the torque difference between the left and right motors [3], [4], [5]. Furthermore, integrated vehicle control methods have been developed using active steering with steer-by-wire systems [6], [7] or body slip angle estimation methods [8], [9]. The authors' group has already proposed yaw-rate control based on a yaw-moment observer (YMO) [10], lateral-force observer [11], and body slip angle estimation using a lateral force sensor [12].

Fig. 1. FPEV2-Kanon.

Fig. 2. In-wheel motor.

In this paper, we focus on the tire workload and propose an advanced yaw-rate control scheme for the situation where a vehicle turns while accelerating or decelerating. Tire workload is the ratio of the current tire force to the maximum tire force that can be generated. As the tire workload approaches unity, the driving and lateral forces saturate, and the vehicle spins while making a turn. Therefore, reducing the workload is important for maintaining a vehicle's lateral stability [13], and a tire force distribution method has been studied for equalizing the tire workload [14]. However, the previous study was not implemented on a real vehicle, and experimental results have not been published.

Additionally, a novel torque distribution method that considers each motor separately is proposed with lateral force control based on active front and rear steering systems. The proposed method has a relatively low computational cost because it is based on the sum of squares minimization problem. Simulations and experiments are carried out using an EV with in-wheel motors to demonstrate that the stability of vehicle lateral motion is greatly enhanced with the proposed method.

II. Experimental Vehicle and Vehicle Model

A. Experimental Vehicle

In this section, characteristics of the experimental EV "FPEV2-Kanon," shown in Fig. 1, are explained. FPEV2-Kanon has been developed by the authors' research group and has been used for control performance verification. The vehicle's specifications are summarized in Table I.

978-1-4799-0224-8/13/$31.00 ©2013 IEEE

TABLE I
VEHICLE SPECIFICATIONS.

Vehicle Mass (M)	870 [kg]
Vehicle Inertia (I)	617.0 [kg $\cdot$ m^2]
Wheel Base (l)	1.7 [m]
Distance from C.G to Front Axle (l_f)	0.999 [m]
Distance from C.G to Rear Axle (l_r)	0.701 [m]
Front Cornering Stiffness (C_f)	11220 [N/rad]
Rear Cornering Stiffness (C_r)	31200 [N/rad]
Tread Base (d_f, d_r)	1.3 [m]
Wheel Radius (r)	0.302 [m]

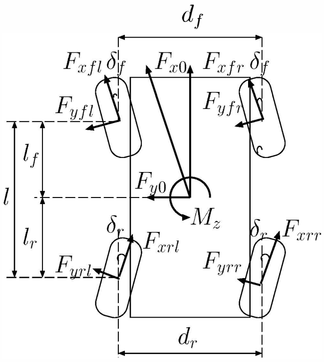

Fig. 3. Vehicle model.

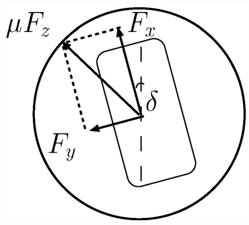

Fig. 4. Friction circle.

Outer-rotor-type in-wheel motors, shown in Fig. 2, are installed in each wheel. Because these motors use a direct drive system, reaction forces from the road are directly transferred to the motors without gear reduction or backlash. The maximum torque of each front motor is ±500 [Nm], and that of each rear motor is ±340 [Nm].

Active front and rear steering systems comprising two 250 W DC motors for electric power steering are used. Additionally, a multi-sensing hub (MSHub) unit, a tire lateral force sensor which is being developed by NSK Ltd., is installed in each wheel for measuring lateral force [12]. Moreover, an optical sensor is installed to accurately measure the vehicle velocity and body slip angle.

B. Vehicle Modeling

In this section, the dynamics of the abovementioned EV is modeled, which has four in-wheel motors that can be driven independently and has active front and rear steering systems [15]. We assume that the steering angles of each front and rear wheel, defined as δ_f and δ_r, are negligibly small. The equations of each longitudinal, lateral, and yawing motion of this vehicle, shown in Fig.3, are written as follows:

$$F_{xfl} + F_{xfr} + F_{xrl} + F_{xrr} = F_{x0}, \quad (1)$$
$$F_{yfl} + F_{yfr} + F_{yrl} + F_{yrr} = F_{y0}, \quad (2)$$
$$-\frac{d_f}{2}F_{xfl} + \frac{d_f}{2}F_{xfr} - \frac{d_r}{2}F_{xrl} + \frac{d_r}{2}F_{xrr} = N_z, \quad (3)$$
$$l_f(F_{yfl} + F_{yfr}) - l_r(F_{yrl} + F_{yrr}) = N_t, \quad (4)$$
$$N_z + N_t = M_z, \quad (5)$$

where the total longitudinal force of the vehicle is denoted by F_{x0}; the longitudinal forces of each wheel are denoted by F_{xfl}, F_{xfr}, F_{xrl}, and F_{xrr}; the total lateral force of the vehicle is denoted by F_{y0}; the lateral forces of each wheel are denoted by F_{yfl}, F_{yfr}, F_{yrl} and F_{yrr}; the yaw moment generated by the longitudinal force of each wheel is denoted by N_z; the yaw moment due to the lateral force of each wheel is denoted by N_t; the total yaw moment of the vehicle is denoted by M_z; the tread bases of the front and rear axles are denoted by d_f and d_r, respectively; and the distances from the vehicle's center of gravity (c.g.) to the front and rear axle treads are denoted by l_f and l_r, respectively.

The shift in the vertical load of each wheel according to the acceleration is modeled as follows:

$$F_{zfl} = \frac{1}{2}\frac{l_r}{l}Mg - \rho_f a_y M\frac{h_g}{d_f} - a_x M\frac{h_g}{l}, \quad (6)$$
$$F_{zfr} = \frac{1}{2}\frac{l_r}{l}Mg + \rho_f a_y M\frac{h_g}{d_f} - a_x M\frac{h_g}{l}, \quad (7)$$
$$F_{zrl} = \frac{1}{2}\frac{l_f}{l}Mg - \rho_r a_y M\frac{h_g}{d_r} + a_x M\frac{h_g}{l}, \quad (8)$$
$$F_{zrr} = \frac{1}{2}\frac{l_f}{l}Mg + \rho_r a_y M\frac{h_g}{d_r} + a_x M\frac{h_g}{l}, \quad (9)$$

where the vertical loads of the wheels are denoted by F_{zfl}, F_{zfr}, F_{zrl}, and F_{zrr}; vehicle weight is denoted by M; wheel base is denoted by l; roll stiffness distribution is denoted by ρ_f and ρ_r; height of the c.g. is denoted by h_g, and the accelerations in the longitudinal and lateral directions are respectively denoted by a_x and a_y.

Moreover, the relation among F_x, F_y, and F_z should satisfy the following equation in any case.

$$\sqrt{F_x^2 + F_y^2} \leq \mu F_z \quad (10)$$

Here, the coefficient of friction is denoted by μ. (10) means that the resultant force of F_x and F_y cannot exceed the maximum friction force μF_z. Then, this vector has to be within a circle of radius μF_z. This circle is called the friction circle and is shown in Fig.4.

Moreover, if the side slip angles of each tire are negligibly small, the vehicle can be modeled as a linear two-wheeled model [15]. In this model, the relation between the lateral force of each wheel and the cornering force, Y_f and Y_r, is approximated as follows:

$$F_{yfl} \simeq F_{yfr} \simeq F_{yf} \simeq Y_f = -C_f\alpha_f = -C_f\left(\beta + \frac{l_f}{V}\gamma - \delta_f\right), \quad (11)$$
$$F_{yrl} \simeq F_{yrr} \simeq F_{yr} \simeq Y_r = -C_r\alpha_r = -C_r\left(\beta - \frac{l_r}{V}\gamma - \delta_r\right), \quad (12)$$

where cornering stiffness is denoted by C_f and C_r (front and rear, respectively), tire side slip angles are denoted by α_f and α_r, vehicle side slip angle is denoted by β, yaw rate is denoted by γ.

III. CONVENTIONAL YAW-RATE CONTROL

A. Yaw-Moment Observer

This section describes a direct yaw-moment control method based on the YMO [10] previously proposed by the authors' research group.

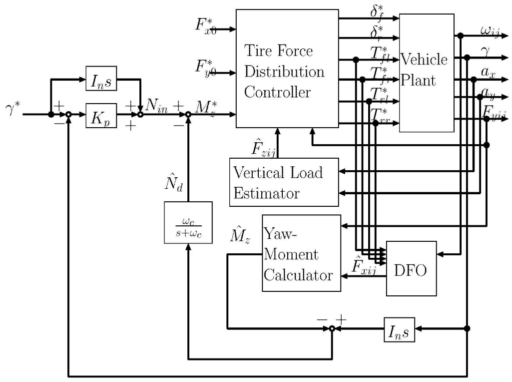

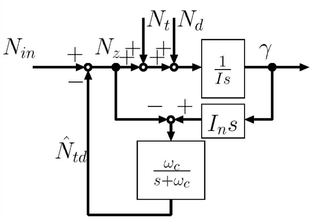

Fig. 5. Block diagram of YMO.

$i = \mathrm{f}, \mathrm{r}, j = \mathrm{l}, \mathrm{r}$
DFO: Driving Force Observer

Fig. 6. Block diagram of yaw-rate control.

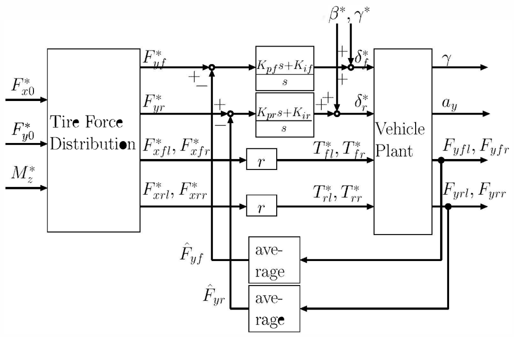

Fig. 7. Block diagram of tire force distribution controller.

From (3)–(5), the yawing dynamics is formulated as follows:

$$I\dot{\gamma} = N_z + N_t + N_d, \tag{13}$$

where vehicle yaw inertia moment is denoted by I and disturbance yaw moment is denoted by N_d. Then, the disturbance observer shown in Fig.5 is composed. This observer compensates for the lumped disturbance $N_{td} := N_t + N_d$ with the control yaw moment N_z, which is generated owing to the torque difference between the left and right motors, and nominalizes the system as follows:

$$\gamma(s) \simeq \frac{1}{I_n s} N_{in}(s). \tag{14}$$

This specific disturbance observer is called the YMO.

B. Conventional YMO-Based Yaw-Rate Control

In this section, a conventional yaw-rate control method with driving and braking force distribution of each wheel is explained. This yaw-rate controller is composed of a feedback (FB) controller, feedforward (FF) controller, and the YMO mentioned in Section III-A. The sum of outputs of the FB and FF controllers is N_{in}. For canceling the disturbance yaw moment, N_{dt}, a control yaw moment, N_z, is generated.

In the conventional method, the front and rear driving forces are distributed equally. The longitudinal force on each wheel can be determined using (1) and (3) as follows:

$$F_{xfl} = F_{xrl} = F_{xl} \tag{15}$$

$$F_{xfr} = F_{xrr} = F_{xr} \tag{16}$$

$$\begin{bmatrix} F_{xl} \\ F_{xr} \end{bmatrix} = \begin{bmatrix} \frac{1}{4} & -\frac{1}{2}\frac{1}{d_f + d_r} \\ \frac{1}{4} & \frac{1}{2}\frac{1}{d_f + d_r} \end{bmatrix} \begin{bmatrix} F_{x0} \\ N_z \end{bmatrix} \tag{17}$$

From (17), the torque command given to each in-wheel motor can be calculated as follows:

$$T^*_{ij} = rF^*_{xj} \ (i = f, r, j = l, r). \tag{18}$$

IV. Proposed Method

A. Least Squares Distribution Method

In this section, a novel yaw-rate control method that uses active front and rear steering systems with driving and braking force distribution of four wheels is proposed. In the proposed method, the disturbance yaw moment, N_d, is estimated from the vehicle yaw moment, M_z, and yaw rate, γ, using a novel YMO, as shown in Fig. 6. For measuring M_z in (5), N_t can be detected using four lateral force sensors, and N_z can be estimated using a driving-force observer [1].

Using the approximation in (11) and (12), (1) – (5) can be rewritten as follows:

$$\begin{bmatrix} 0 & 0 & 1 & 1 & 1 & 1 \\ 2 & 2 & 0 & 0 & 0 & 0 \\ 2l_f & -2l_r & -\frac{d_f}{2} & \frac{d_f}{2} & -\frac{d_r}{2} & \frac{d_r}{2} \end{bmatrix} \begin{bmatrix} F_{yf} \\ F_{yr} \\ F_{xfl} \\ F_{xfr} \\ F_{xrl} \\ F_{xrr} \end{bmatrix} = \begin{bmatrix} F_{x0} \\ F_{y0} \\ M_z \end{bmatrix}, \tag{19}$$

where the left-hand side coefficient matrix is denoted by A, vector of lateral and longitudinal forces on each wheel is denoted by $x = [F_{yf}\ F_{yr}\ F_{xfl}\ F_{xfr}\ F_{xrl}\ F_{xrr}]^T$, and right-hand vector is denoted by $b = [F_{x0}\ F_{y0}\ M_z]^T$. The workload on each wheel, which is the rate of the resultant force in the friction circle, is defined as follows:

$$\eta_{fl} = \frac{\sqrt{F_{xfl}^2 + F_{yfl}^2}}{\mu_{\max} F_{zfl}} \simeq \frac{\sqrt{F_{xfl}^2 + F_{yf}^2}}{\mu_{\max} F_{zfl}}, \tag{20}$$

$$\eta_{fr} = \frac{\sqrt{F_{xfr}^2 + F_{yfr}^2}}{\mu_{\max} F_{zfr}} \simeq \frac{\sqrt{F_{xfr}^2 + F_{yf}^2}}{\mu_{\max} F_{zfr}}, \tag{21}$$

$$\eta_{rl} = \frac{\sqrt{F_{xrl}^2 + F_{yrl}^2}}{\mu_{\max} F_{zrl}} \simeq \frac{\sqrt{F_{xrl}^2 + F_{yr}^2}}{\mu_{\max} F_{zrl}}, \tag{22}$$

$$\eta_{rr} = \frac{\sqrt{F_{xrr}^2 + F_{yrr}^2}}{\mu_{\max} F_{zrr}} \simeq \frac{\sqrt{F_{xrr}^2 + F_{yr}^2}}{\mu_{\max} F_{zrr}}, \tag{23}$$

where the maximum value of the friction coefficient is denoted by $\mu_{\max}$. Under the assumption that the $\mu_{\max}$ values of all wheels are equal, the performance index J is defined as the sum of the squares of the individual wheels' workloads as follows:

$$\begin{aligned} J &= \sum_{i=f,r}\sum_{j=l,r}(\mu_{\max}\eta_{ij})^2 \\ &= \frac{F_{xfl}^2+F_{yf}^2}{F_{zfl}^2}+\frac{F_{xfr}^2+F_{yf}^2}{F_{zfr}^2}+\frac{F_{xrl}^2+F_{yr}^2}{F_{zrl}^2}+\frac{F_{xrr}^2+F_{yr}^2}{F_{zrr}^2} \\ &= x^TWx \qquad (24) \\ W &= \mathrm{diag}\left(\frac{1}{F_{zfl}^2}+\frac{1}{F_{zfr}^2},\frac{1}{F_{zrl}^2}+\frac{1}{F_{zrr}^2},\frac{1}{F_{zfl}^2},\frac{1}{F_{zfr}^2},\frac{1}{F_{zrl}^2},\frac{1}{F_{zrr}^2}\right) \qquad (25) \end{aligned}$$

The weighted least squares solution x_{opt} with respect to (19) for minimizing the cost function J can be written as follows:

$$x_{opt} = W^{-1}A^T(AW^{-1}A^T)^{-1}b \qquad (26)$$

A block diagram of tire force distribution controller is shown in Fig.7. For generating the distributed longitudinal force on each wheel, the torque command to the in-wheel motors is calculated as follows:

$$T_{ij}^* = rF_{xij}^* \ (i=f,r,j=l,r). \qquad (27)$$

B. Lateral Force Feedback Control

In this section, a control method for the lateral force on each front and rear wheel is explained, which is shown in Fig. 7.

In the domain of $|\alpha| \ll 1$, where the lateral force F_y is assumed to be a linear function of side-slip angle α, the transfer function from α to F_y is a first-order system [15]. Therefore, for tracking the lateral-force commands F_{yi}^* $(i = f,r)$ obtained in (26), the lateral forces are controlled by a proportional-integral controller using the outputs of the lateral force sensors F_{yij}, which is designed by the pole assignment method with the following first-order plant.

$$\frac{F_{yf}(s)}{\alpha_f(s)} = -C_f\frac{1}{\tau_y s+1} \qquad (28)$$

$$\frac{F_{yr}(s)}{\alpha_r(s)} = -C_r\frac{1}{\tau_y s+1} \qquad (29)$$

V. SIMULATION

A. Simulation Setup

For confirming the effectiveness of the proposed workload equalization scheme, simulations of cornering under braking were carried out using MATLAB/Simulink.

Each constant of the EV is listed in Table I. The height of the c.g. was set to $h_g = 0.454$ [m] and the roll stiffness distribution was simply assumed as $\rho_f = \rho_r = 0.5$. The friction coefficient was defined as $\mu_{\max} = 0.7$.

In the controllers, the proportional gain in the yaw-rate feedback controller, which is defined as K_p, was designed by the pole placement to the closed-loop pole at -5 [rad/s], in which the nominal plant model is $\frac{\gamma}{N_{in}} = \frac{1}{I_n s}$. Then, the poles of the lateral force PI controller are set to $\omega_f = -4.5$ [rad/s] and $\omega_r = -2$ [rad/s].

In simulations, the conventional method is the YMO-based yaw-rate control scheme mentioned in Section III-B, and the proposed method is the yaw-rate control with the proposed YMO and the weighted least squares (WLS) method mentioned in Section IV-A. Simulations start with a vehicle speed of 30 [km/h]; then at 1 [s], a front steering angle reference $\delta^* = 0.06$ [rad] is input. Further, at 3 s, a vehicle longitudinal force reference $F_{x0}^* = -1000$ [N] is input.

Yaw-rate control and tire force distribution starts when the front wheel steering angle reference δ^* is input. Each yaw rate and vehicle lateral force command is decided from the values when the front steering angle reference δ^* is input into a neutral steer (NS) vehicle. That is, the yaw-rate reference is decided as a NS vehicle's steady-state value $\gamma^* = \frac{V}{l}\delta^*$. For setting the vehicle lateral acceleration to the NS vehicle steady-state value $a_y^* = \frac{V^2}{l}\delta^*$, the vehicle lateral force command is determined to be $F_{y0}^* = Ma_y^*$.

B. Simulation Results

The simulation results are shown in Figs. 8 and 9. In these figures, Fig. 8 shows the results of the conventional method, and Fig. 9 shows those of the proposed method.

Fig. 9(a) indicates that the front and rear steering angles, δ_f, δ_r, respectively, are distributed according to the proposed method, while the conventional method generates only the front steering angle δ_f, which is the same value as the driver's steering input δ_h^*, as shown in Fig. 8(a). Then, as can be seen in Figs. 8(b) and 9(b), both methods generate driving force of each wheel to ensure that the yaw rate corresponds to the reference, as shown in Figs. 8(c) and Fig. 9(c).

Figures 8(d) and 9(d) show the tire workload on each wheel. The rear-left tire workload reaches its maximum value as soon as the vehicle starts decelerating because the tire vertical load leans to right while cornering to the left, and, in addition, shifts from the rear to the front during deceleration. Consequently, the rear-left tire workload is as much as 0.65 in the conventional method, as shown in Fig. 8(d). In contrast, the proposed method succeeds in reducing the tire workload to 0.5, as shown in Fig. 9(d). If the tire workload reaches 1, the driving and lateral forces cannot be generated any more, thus leading to tire slip or wheelspin. Therefore, the result implies that the proposed method improves vehicle safety during deceleration and cornering.

Figures 9(e) and 9(f) show the front and rear lateral forces under the proposed control method. It can be seen that the lateral forces are well controlled to track the reference values by the PI controller.

VI. EXPERIMENT

A. Experiment Setup

For demonstrating the effectiveness of the proposed method, experiments on yaw-rate control under braking were carried out. In these experiments, the constants and parameters were identical to those in Section V.

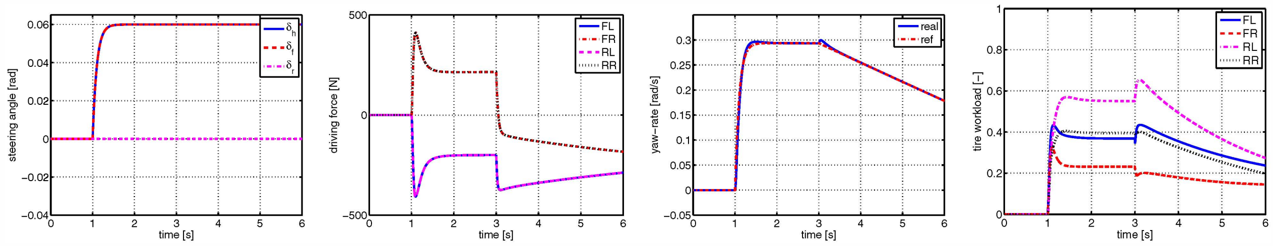

(a) Front/rear steering angle. (b) Driving force on each wheel. (c) Yaw-rate. (d) Tire workload on each wheel.

Fig. 8. Simulation result (conventional method using YMO).

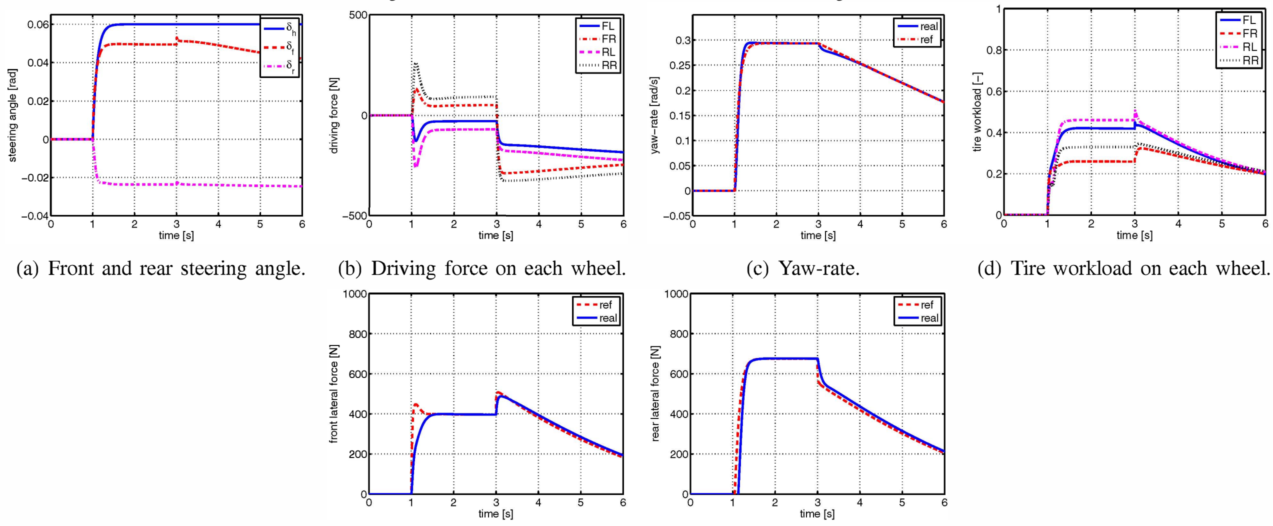

(a) Front and rear steering angle. (b) Driving force on each wheel. (c) Yaw-rate. (d) Tire workload on each wheel.

(e) Front lateral force. (f) Rear lateral force.

Fig. 9. Simulation result (proposed method using YMO and WLS).

The vehicle was accelerated to 30 [km/h]. Then, front wheel steering angle reference $\delta^* = 0.06$ [rad] was input. In addition, vehicle longitudinal force reference $F_{x0}^* = -1000$ [N] was input. Yaw-rate control and tire force distribution were switched on when the front wheel steering angle reference δ^* was input. All yaw-rate and vehicle lateral force reference values were identical to those in the simulations.

B. Experiment Results

The experimental results are shown in Figs. 10 and 11. Fig. 10 shows the results of the conventional method, while Fig. 11 shows those of the proposed method.

The front and rear steering angles, shown in Figs. 10(a) and 11(a), and the driving force of each wheel shown in Fig. 10(b) and 11(b), are almost the same as those in the simulation results V-B. As for the yaw rate, it follows the reference for the most part, as shown in Figs. 10(c) and 11(c), while tracking performance of the proposed method is slightly worse than that of the simulation. This can possibly be ascribed to the proportional gain K_p of the yaw-rate feedback controller being too small and the disturbance rejection performance being restricted.

Figures 10(d) and 11(d) show the tire workload on each wheel. The rear-left tire workload approaches unity in the conventional method, as shown in Fig. 10(d). In contrast, the proposed method reduces the tire workload to 0.4, as can be seen in Fig. 11(d), which means that vehicle safety is drastically improved.

Figures 11(e) and 11(f) show the front and rear lateral forces under the proposed control method. It can be seen that the lateral forces are well controlled by the PI controller to follow the references.

VII. Conclusion

This paper presents an integrated vehicle motion control scheme through lateral force control and longitudinal and lateral force distributions based on a least-squares solution. The effectiveness of the proposed method is verified through simulations and experiments.

Compared to the conventional method, the proposed method can equalize tire workload on each wheel as well as control the yaw rate such that they follow their respective reference values. Given that tire forces can be prevented from reaching saturation by decreasing the tire workload on each wheel, vehicle stability and safety is improved during acceleration, deceleration, and cornering.

Acknowledgment

The authors wish to thank the first author's former students, Mr. Ando for the helps in simulations. This research was

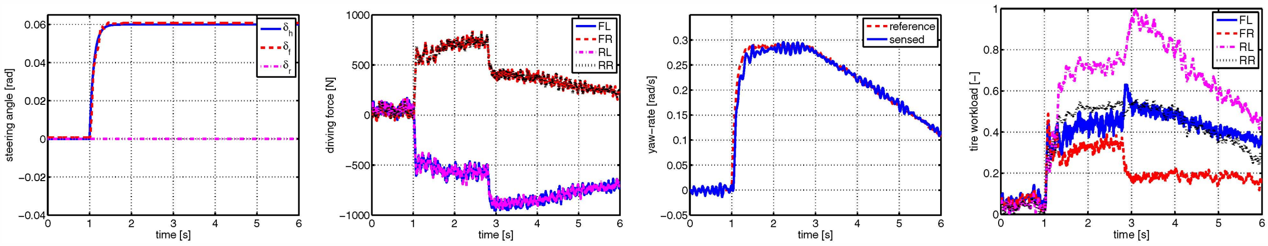

(a) Front/rear steering angle. (b) Driving force on each wheel. (c) Yaw-rate. (d) Tire workload on each wheel.

Fig. 10. Experimental result (conventional method using YMO).

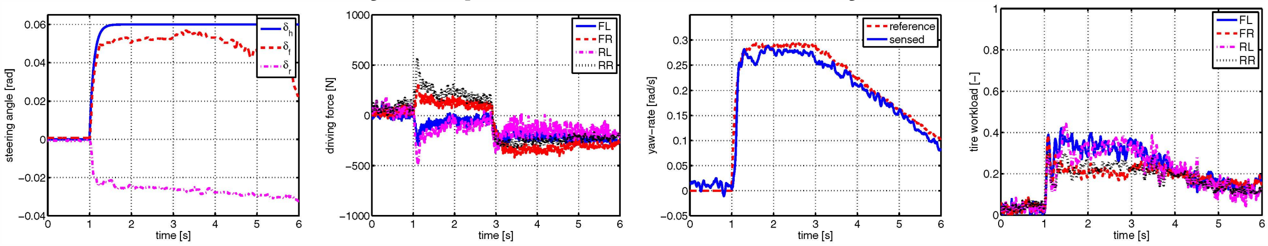

(a) Front/rear steering angle. (b) Driving force on each wheel. (c) Yaw-rate. (d) Tire workload on each wheel.

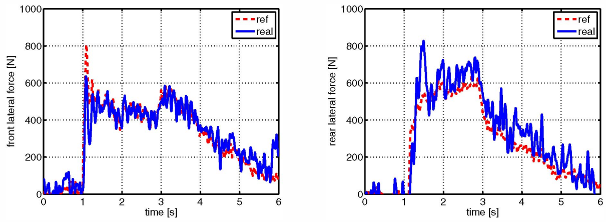

(e) Front lateral force. (f) Rear lateral force.

Fig. 11. Experimental result (proposed method using YMO and WLS).

partly supported by the Industrial Technology Research Grant Program from the New Energy and Industrial Technology Development Organization (NEDO) of Japan (No. 05A48701d) and by the Ministry of Education, Culture, Sports, Science and Technology through grant (No. 22246057). In addition, we would like to thank NSK Ltd. for offering the multi-sensing hub (MSHub) tire lateral-force sensors.

REFERENCES

[1] Y. Hori, "Future vehicle driven by electricity and control—research on four-wheel-motored "uot electric march ii"," *IEEE Transactions on Industrial Electronics*, vol. 51, no. 5, pp. 954–962, 2004.

[2] H. Imine, L. M. Fridman, and T. Madani, "Steering control for rollover avoidance of heavy vehicles," *IEEE Transactions on Vehicular Technology*, vol. 61, no. 8, pp. 3499–3509, 2012.

[3] J. Kim, C. Park, S. Hwang, Y. Hori, and H. Kim, "Control algorithm for an independent motor-drive vehicle," *IEEE Transactions on Vehicular Technology*, vol. 59, no. 7, pp. 3213–3222, 2010.

[4] J. Kang, J. Yoo, and K. Yi, "Driving control algorithm for maneuverability, lateral stability, and rollover prevention of 4wd electric vehicles with independently driven front and rear wheels," *IEEE Transactions on Vehicular Technology*, vol. 60, no. 7, pp. 2987–3001, 2011.

[5] S. Yim, J. Choi, and K. Yi, "Coordinated control of hybrid 4wd vehicles for enhanced maneuverability and lateral stability," *IEEE Transactions on Vehicular Technology*, vol. 61, no. 4, pp. 1946–1950, 2012.

[6] Y. Yamaguchi and T. Murakami, "Adaptive control for virtual steering characteristics on electric vehicle using steer-by-wire system," *IEEE Transactions on Industrial Electrinics*, vol. 56, no. 5, pp. 1585–1594, 2009.

[7] A. E. Cetin, M. A. Adli, D. E. Barkana, and H. Kucuk, "Implementation and development of an adaptive steering-control system," *IEEE Transactions on Vehicular Technology*, vol. 59, no. 1, pp. 75–83, 2010.

[8] W. Cho, J. Yoon, S. Yim, B. Koo, and K. Yi, "Estimation of tire slip angle and friction limits using steering torque," *IEEE Transactions on Vehicular Technology*, vol. 59, no. 2, pp. 638–649, 2010.

[9] S. Han and K. Huh, "Monitoring system design for lateral vehicle motion," *IEEE Transactions on Vehicular Technology*, vol. 60, no. 4, pp. 1394–1403, 2011.

[10] H. Fujimoto, T. Saito, and T. Noguchi, "Motion stabilization control of electric vehicle under snowy conditions based on yaw-moment observer," in *Proceedings of The 8th IEEE International Workshop on Advanced Motion Control*, pp. 35–40, 2004.

[11] Y. Yamauchi and H. Fujimoto, "Advanced motion control of electric vehicle based on lateral force observer with active steering," in *Proceedings of 2010 IEEE International Symposium on Industrial Electronics*, pp. 3627–3632, 2010.

[12] K. Nam, S. Oh, H. Fujimoto, and Y. Hori, "Estimation of sideslip and roll angles of electric vehicles using lateral tire force sensors through rls and kalman filter approaches," *IEEE Transactions on Industrial Electronics*, vol. 60, no. 3, pp. 988–1000, 2013.

[13] E. Ono, Y. Hattori, H. Aizawa, H. Kato, S. Tagawa, and S. Niwa, "Clarification and achievement of theoretical limitation in vehicle dynamics integrated management," *Journal of Environment and Engineering*, vol. 4, no. 1, pp. 89–100, 2009.

[14] A. Roshanbin and M. Naraghi, "Vehicle integrated control-an adaptive optimal approach to distribution of tire forces," in *Proceedings of The IEEE International Conference on Networking, Sensing and Control, 2008*, pp. 885–890, 2008.

[15] M. Abe, *Vehicle Handling Dynamics*. Butterworth-Heinemann, 2009.